

STATICS OF POINT JOSEPHSON JUNCTIONS IN A MICRO STRIP LINE.

J.G. CAPUTO* AND L. LOUKITCH †

Abstract. We model the static behavior of point Josephson junctions in a micro strip line using a 1D linear differential equation with delta distributed sine non-linearities. We analyze the maximum current γ_{max} crossing the micro strip for a given magnetic field H . In particular we establish its periodicity and analyze how it is affected by the geometry, length, type of current feed, position and area of the junctions. For small currents, which is the rule in practice, we show that γ_{max} can be obtained by a simple formula, the magnetic approximation. This model is in excellent agreement with measurements obtained for real devices.

Key words. Josephson junctions, sine gordon equation, Dirac delta function, Optimization

AMS subject classifications. 35Qxx Equations of Mathematical physics
35Jxx Boundary value problems elliptic equations
46Fxx Distributions, Generalized function

1. Introduction. The coupling of two low T_c superconductors across a thin oxide layer is described by the Josephson equations [1].

$$(1.1) \quad V = \Phi_0 \frac{d\phi}{dt}, \quad I = sJ_c \sin(\phi),$$

where V and I are, respectively, the voltage and current across the barrier, s is the contact surface, J_c is the critical current density and $\Phi_0 = \hbar/2e$ is the reduced flux quantum. These two Josephson relations together with Maxwell's equations imply the modulation of DC current by an external magnetic field in the static regime and the conversion of AC current into microwave radiation [2, 3]. Other applications include Rapid single flux quantum logic electronics[3] and microwave signal mixers used in integrated receivers for radio-astronomy[4]. In all these systems there is a characteristic length which reduces to the Josephson length, λ_J , the ratio of the electromagnetic flux to the quantum flux Φ_0 for standard junctions.

For many applications and in order to protect the junction, Josephson junctions are embedded in a so called microstrip line which is the capacitor made by the overlap of the two superconducting layers. This is the so-called "window geometry" where the phase difference between the top and bottom layer satisfies an inhomogeneous 2D damped driven sine Gordon equation [5] resulting from Maxwell's equations and the Josephson constitutive relations (1.1). The damping is due to the normal electrons and the driving through the boundary conditions with an external current or magnetic field applied to the device.

Even in the static regime the 2D problem is complicated because of the multiplicity of solutions due to the sine term. However flux penetration occurs along the direction of the magnetic field so one direction dominates the other. A quantity measured by experimentalists is the maximum (static) current $I_{max}(H)$ that can cross the device for a given magnetic field H . This gives informations on the quality of the

*Laboratoire de Mathématiques, Institut de Sciences Appliquées, B.P. 8, 76131 Mont-Saint-Aignan Cedex, France and Laboratoire de Physique théorique et modélisation, Université de Cergy-Pontoise and C.N.R.S.

†Laboratoire de Mathématiques, Institut de Sciences Appliquées, B.P. 8, 76131 Mont-Saint-Aignan Cedex, France.

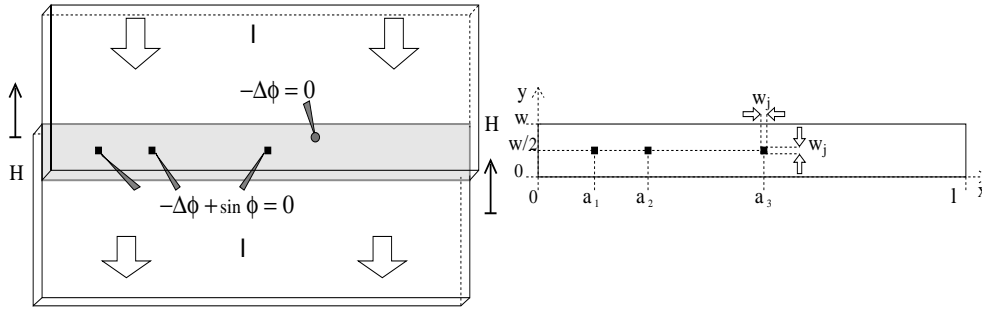


FIG. 1.1. The left panel shows the top view of a superconducting microstrip line containing three Josephson junctions, H, I and ϕ are respectively the applied magnetic field, current and the phase difference between the two superconducting layers. The phase difference ϕ between the two superconducting layers satisfies $-\Delta\phi = 0$ in the linear part and $-\Delta\phi + \sin(\phi) = 0$ in the Josephson junctions. The right panel shows the associated 2D domain of size $l \times w$ containing $n = 3$ junctions placed at the positions $y = w/2$ and $x = a_i$, $i = 1, n$.

junctions. An important issue is how defects in the coupling will affect this maximum current. In particular high T_c superconductors can be described as Josephson junctions where the critical current density is a rapidly varying function of the position, due to grain boundaries. Fehrenbacher et al[13] calculated $I_{\max}(H)$ for such disordered long Josephson junctions and for a periodic array of defects. Experiments were also done by Itzler and Tinkham on large 2D disordered junctions [14]. However the overall picture is complex and it is difficult from the curve $I_{\max}(H)$ to obtain geometric information on the junction. The analysis of such a 2D problem [11] provided bounds on the gradient of the solution that were independent of the area of the junctions so that little information could be obtained on $I_{\max}(H)$. However the study [11] proved the existence of solutions and the convergence of the Picard iteration to obtain them.

Small junctions of length $w_i < \lambda_J$ are easier to study and lead to the well known $I_{\max}(H) = \sin(Hw_i)/H$ [2]. Two such junctions are commonly associated to form a Superconducting Quantum Interference Device (SQUID) now routinely used to measure magnetic fields. More junctions can be used to form arrays [12] that can bear more critical current and are more flexible than a long junction because the area of the junction components and their position can be varied. When the junctions are closer than λ_J , such arrays behave as a long junction and could be used as microwave generators. Almost all models are discrete lumped models where the effect of the space between junctions is neglected. In particular the interaction of the junctions through this passive region has always been neglected. This makes it difficult to describe junctions of different areas, placed non uniformly in the microstrip. This is why up to now mostly equidistant and identical junctions have been considered. To overcome these difficulties we recently introduced a continuous/discrete model that preserves the continuity of the phase and its normal gradient across the junction interface and where the phase is assumed constant in the junctions. The 1D dynamics [9] of one junction in a cavity revealed that the junction could stop waves across the cavity or enhance them throughout. In [8] this model was used to calculate $I_{\max}(H)$ for a miss-aligned SQUID in a 2D cavity. Nonuniform arrays of junctions that are generalized SQUIDs have been produced and analyzed in particular by Salez et al at the Observatory of Paris[4] and our analysis is in excellent agreement with the

measured $I_{\max}(H)$.

In this article we will concentrate on the 1D static problem and show that it allows for an in depth analysis that was out of reach in the general 2D case. In particular we will show the properties of $I_{\max}(H)$, its periodicity, its regularity, the relation between different types of current feeds and how it is affected by the position of the array in the microstrip. In addition we introduce and justify the so-called magnetic approximation where many details of $I_{\max}(H)$ can be controlled. Specifically in section two we introduce our model and give preliminary analytical results in section three. Section four details the intrinsic properties of the maximal current as a function of the magnetic field: its periodicity, the relation between the inline and overlap current feed and the simple magnetic approximation. Section five introduces two numerical ways to solve the problem. In the sixth section, we study a SQUID and examine the effect of a little difference between the junction parameters and we compare this to the experiment. Section seven deals with devices with more junctions, there we analyze the effect of separating one junction from the others and show the agreement with the experimental results.

2. The model. The device we model shown in Fig. 1.1 is a so-called microstrip cavity (grey area in Fig. 1.1) between two superconducting layers. Inside this microstrip there are regions where the oxide layer is very thin (~ 10 Angstrom) enabling Josephson coupling between the top and bottom superconductors. The dimensions of the microstrip are about $100 \mu\text{m}$ in length and $20 \mu\text{m}$ in width. The phase difference between the top and bottom superconducting layers obeys in the static regime the following semilinear elliptic partial differential equation [5]

$$(2.1) \quad -\Delta\varphi + g(x, y) \sin \varphi = 0,$$

where $g(x, y)$ is 1 in the Josephson junctions and 0 outside. This formulation guarantees the continuity of the normal gradient of φ , the electrical current on the junction interface. The unit of space is the Josephson length λ_J , the ratio of the flux formed with the critical current density and the surface inductance to the flux quantum Φ_0 .

The boundary conditions representing an external current input I or an applied magnetic field H (along the y axis) are

$$(2.2) \quad \begin{aligned} \frac{\partial\varphi}{\partial y}\Big|_{y=0} &= -\frac{I}{2l}\nu, & \frac{\partial\varphi}{\partial y}\Big|_{y=w} &= \frac{I}{2l}\nu, \\ \frac{\partial\varphi}{\partial x}\Big|_{x=0} &= H - \frac{I}{2w}(1-\nu), & \frac{\partial\varphi}{\partial x}\Big|_{x=l} &= H + \frac{I}{2w}(1-\nu), \end{aligned}$$

where $0 \leq \nu \leq 1$ gives the type of current feed. The case $\nu = 1$ shown in Fig. 1.1 where the current is only applied to the long boundaries $y = 0, w$ is called overlap feed while $\nu = 0$ corresponds to the inline feed.

We consider long and narrow strips containing a few small junctions of size $w_j \times w_j$ placed on the line $y = w/2$ and centered on $x = a_i$, $i = 1, n$ as shown in Fig. 1.1. We then search φ in the form

$$(2.3) \quad \varphi(x, y) = \frac{\nu I}{2L} \left(y - \frac{\omega}{2}\right)^2 + \sum_{n=0}^{+\infty} \phi_n(x) \cos\left(\frac{n\pi y}{w}\right),$$

where the first term takes care of the y boundary condition. For narrow strips $w < \pi$, only the first transverse mode needs to be taken into account [6, 7] because the

curvature of φ due to current remains small. Inserting (2.3) into (2.1) and projecting on the zero mode we obtain the following equation for ϕ_0 where the 0's have been dropped for simplicity

$$(2.4) \quad -\phi'' + g\left(x, \frac{w}{2}\right) \frac{w_j}{w} \sin \phi = \nu \frac{\gamma}{l},$$

where $\gamma = I/w$ and the boundary conditions $\phi'(0) = H - (1 - \nu)\gamma/2$, and $\phi'(l) = H + (1 - \nu)\gamma/2$.

As the area of the junction is reduced, the total Josephson current is reduced and tends to zero. To describe small junctions where the phase variation can be neglected but that can carry a significant current, we introduce the following function g_h

$$(2.5) \quad g_h(x) = \frac{w_j}{2h} \quad \text{for } a_i - h < x < a_i + h, \quad g_h(x) = 0 \quad \text{elsewhere,}$$

where $i = 1, \dots, n$. In the limit $h \rightarrow 0$ we obtain our final delta function model [9]

$$(2.6) \quad -\phi'' + \sum_{i=1}^n d_i \delta(x - a_i) \sin \phi = \nu j,$$

where

$$(2.7) \quad d_i = \frac{w_j^2}{w}, \quad j = \frac{\gamma}{l}$$

and the boundary conditions are

$$(2.8) \quad \phi'(0) = H - (1 - \nu)\gamma/2, \quad \phi'(l) = H + (1 - \nu)\gamma/2.$$

This is our continuous/discrete 1D model of a parallel array of many point Josephson junctions embedded in micro strip cavity. It preserves the spatial degrees of freedom in the linear cavity and the matching conditions at the junction interfaces.

3. General properties. The delta function seems to be a theoretical way to approach the problem. Nevertheless we will show that it provides an excellent agreement with experiments, in addition to allow simple calculations. We have the following properties.

1. Integrating twice (2.6) shows that the solution ϕ is continuous at the junctions $x = a_i$, $i = 1, \dots, n$.
2. Let ϕ be a solution of the equation (2.6), then $\phi + 2k\pi$ is also a solution.
3. Almost everywhere, $-\phi''(x) = \nu\gamma/l$, so that outside the junctions, ϕ is a second degree polynomial by parts,

$$(3.1) \quad \phi(x) = -\frac{\nu j}{2} x^2 + B_i x + C_i, \quad \forall x \in]a_i, a_{i+1}[.$$

4. At each junction ($x = a_i$), ϕ' is not defined, but choosing $\epsilon_1 > 0$, and $\epsilon_2 > 0$, we get

$$\lim_{\epsilon_1 \rightarrow 0} \lim_{\epsilon_2 \rightarrow 0} \int_{a_i - \epsilon_1}^{a_i + \epsilon_2} \phi''(x) dx = \int_{a_i^-}^{a_i^+} \phi''(x) dx = [\phi'(x)]_{a_i^-}^{a_i^+}.$$

Since the phase is continuous at the junction $x = a_i$, we obtain:

$$(3.2) \quad [\phi'(x)]_{a_i^-}^{a_i^+} = d_i \sin(\phi_i),$$

with $\phi_i \equiv \phi(a_i)$.

5. Integrating (2.6) over the whole domain,

$$[\phi']_0^l = \int_0^l \phi'' dx = \sum_{i=1}^n d_i \sin(\phi_i) - \nu\gamma ,$$

and taking into account the boundary conditions, we obtain

$$(3.3) \quad \gamma = \sum_{i=1}^n d_i \sin(\phi_i) ,$$

which indicates the conservation of current. Note that the total current is equal to the sum of the jumps of ϕ' .

3.1. Polynomial by part. Let ϕ be a solution of (2.6) and $\phi_1 = \phi(a_1)$. From remark (3.1), ϕ is a polynomial by parts. We define $P_{i+1}(x)$ the second degree polynomial such that $P_{i+1}(x) = \phi(x)$ for $a_i \leq x \leq a_{i+1}$. Using the left boundary condition we can specify ϕ on $[0, a_1]$:

$$(3.4) \quad P_1(x) = -\frac{\nu j}{2}(x^2 - a_1^2) + \left(H - \frac{1-\nu}{2}\gamma\right)(x - a_1) + \phi_1 .$$

At the junctions (3.2) tells us that $\forall k \in \{1, \dots, n\}$,

$$(3.5) \quad P'_{k+1}(a_k) - P'_k(a_k) = d_k \sin(P_k(a_k)).$$

Considering that $\phi'' = -\nu j$ on each interval, the previous relation and the continuity of the phase at the junction, we can give a first expression for P_{k+1} ,

$$(3.6) \quad P_{k+1}(x) = -\frac{\nu j}{2}(x - a_k)^2 + [P'_k(a_k) + d_k \sin P_k(a_k)](x - a_k) + P_k(a_k).$$

Notice that $P_{k+1}(x)$ depends on $P_k(x)$, ν , j and H . The parameters ν and l are fixed by the geometry of the device. So by recurrence we see that ϕ is entirely determined by the values of ϕ_1 , γ and H .

From (3.5) we can obtain another expression for P_{k+1}

$$(3.7) \quad P_{k+1}(x) - P_k(x) = d_k \sin(P_k(a_k))(x - a_k).$$

Summing all these relations yields

$$(3.8) \quad P_{k+1}(x) = P_1(x) + \sum_{i=1}^k d_i \sin(P_i(a_i))(x - a_i).$$

Polynomials (3.4) and (3.6) show by construction, that the constants H , j and ϕ_1 , determine completely the solution of (2.6) if it exists. In same way, we can show that the three other constants, j , $\phi'(a_1)$ and ϕ_1 fix ϕ . From (3.8), we give an expression of ϕ

$$\phi(x) = P_1(x) + \sum_{i=1}^n \mathcal{H}_{\{x \geq a_i\}} d_i \sin(\phi_i)(x - a_i),$$

where $\mathcal{H}_{\{x \geq a_i\}} = \begin{cases} 1, & x \geq a_i, \\ 0, & x < a_i. \end{cases}$ is the Heaviside function.

3.2. An n th order transcendental system. Another way to solve (2.6) for ϕ is to write it as a coupled system of n transcendental equations. For that, we first eliminate the constant term by introducing ψ such that

$$\phi = \psi - \nu \frac{\gamma}{l} \frac{x^2}{2} \equiv \psi - f(x)$$

and obtain

$$(3.9) \quad -\psi'' + \sum_{i=1}^n d_i \delta(x - a_i) \sin(\psi - f(a_i)) = 0,$$

with the boundary conditions

$$\psi'(0) = H - (1 - \nu)\gamma/2, \quad \psi'(l) = H + (1 + \nu)\gamma/2.$$

To simplify the notation we will write $f_i \equiv f(a_i)$ and $\psi_i \equiv \psi(a_i)$. Integrating (3.9) over the intervals $[0, a_2^-]$, $[a_1^+, a_3^-]$, .. we obtain the relations

$$(3.10) \quad \begin{aligned} -[\psi']_0^{a_2^-} + d_1 \sin(\psi_1 - f_1) &= 0, \\ -[\psi']_{a_1^+}^{a_3^-} + d_2 \sin(\psi_2 - f_2) &= 0, \\ -[\psi']_{a_2^+}^{a_4^-} + d_3 \sin(\psi_3 - f_3) &= 0, \\ -[\psi']_{a_3^+}^{a_5^-} + d_4 \sin(\psi_4 - f_4) &= 0, \\ -[\psi']_{a_4^+}^l + d_5 \sin(\psi_5 - f_5) &= 0, \end{aligned}$$

where we have assumed $n = 5$ as an example. Now we can use the fact that $\psi'' = 0$ in the intervals between the junctions and the boundary conditions to obtain the final system

$$(3.11) \quad \begin{aligned} H - (1 - \nu) \frac{\gamma}{2} - \frac{\psi_2 - \psi_1}{a_2 - a_1} + d_1 \sin(\psi_1 - f_1) &= 0, \\ -\frac{\psi_3 - \psi_2}{a_3 - a_2} + \frac{\psi_2 - \psi_1}{a_2 - a_1} + d_2 \sin(\psi_2 - f_2) &= 0, \\ -\frac{\psi_4 - \psi_3}{a_4 - a_3} + \frac{\psi_3 - \psi_2}{a_3 - a_2} + d_3 \sin(\psi_3 - f_3) &= 0, \\ -\frac{\psi_5 - \psi_4}{a_5 - a_4} + \frac{\psi_4 - \psi_3}{a_4 - a_3} + d_4 \sin(\psi_4 - f_4) &= 0, \\ -H - (1 + \nu) \frac{\gamma}{2} + \frac{\psi_5 - \psi_4}{a_5 - a_4} + d_5 \sin(\psi_5 - f_5) &= 0. \end{aligned}$$

We will use this formulation as well as the one in the previous subsection to establish properties of the solutions and solve the problem numerically using Newton's method.

4. General properties of $\gamma_{max}(H)$ for an n junction array. The general problem is

$$(4.1) \quad -\phi''(x) + \sum_{i=1}^n d_i \delta(x - a_i) \sin(\phi) = \nu j.$$

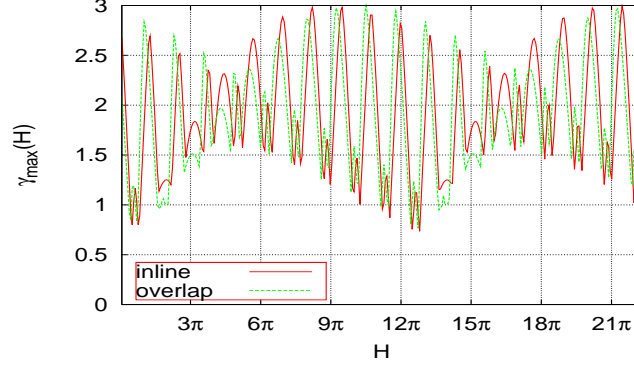


FIG. 4.1. $\gamma_{max}(H)$ curve for an inline current feed, $\nu = 0$ (continuous line) and overlap feed $\nu = 1$ (dotted line) for a three junction unit $\{1, 5/2, 5/2 + 5/3\}$, with $d_1 = d_2 = d_3 = 1$. So $l_1 = 3/2$ and $l_2 = 5/3$.

with the boundary conditions

$$\phi'(0) = H - (1 - \nu)\gamma/2, \quad \phi'(l) = H + (1 - \nu)\gamma/2.$$

Experimentalists measure the maximum current γ for a given magnetic field H and plot this as a curve $\gamma_{max}(H)$. To compare with real data it is therefore important to compute and analyze this quantity. In this section, we give some properties of the $\gamma_{max}(H)$ curve. In the appendix some analytical estimates on the influence of the geometry on the maximal current will be presented.

4.1. Periodicity. We introduce

$$l_j \equiv a_{j+1} - a_j,$$

the distance between two consecutive junctions. Let l_{min} be the smallest distance l_j . We define the array as harmonic if l_i is a multiple of l_{min} for all i .

PROPOSITION 4.1 (Periodicity of the device). *For a harmonic array, the $\gamma_{max}(H)$ curve is periodic with a period $2\pi/l_{min}$.*

Proof. Let ϕ be a solution of (4.1) for a current γ and a magnetic field H . We introduce $f(x) = (2\pi/l_{min})(x - a_1)$ and $\psi(x) = \phi(x) + f(x)$. So ψ verifies

$$(4.2) \quad -\psi''(x) + \sum_{i=1}^n \delta(x - a_i) \sin(\psi - f) = \nu j.$$

with $\psi'(0) = H + 2\pi/l_i - (1 - \nu)\gamma/2$, and $\psi'(l) = H + 2\pi/l_i + (1 - \nu)\gamma/2$. Since, $f(a_j) = 2k\pi$, $\forall i \in \{1, \dots, n\}$, then ψ is a solution of (4.1) for $H + H_p \equiv H + 2\pi/l_{min}$ and the same γ , so $\gamma_{max}(H + H_p) \geq \gamma_{max}(H)$.

Conversely, by subtracting f from a solution associated to $H + H_p$ and a current γ , we obtain a solution for H and the same current γ so $\gamma_{max}(H + H_p) \leq \gamma_{max}(H)$. From the two inequalities we get

$$(4.3) \quad \gamma_{max}(H + H_p) = \gamma_{max}(H) .$$

with $H_p = 2\pi/l_{min}$. \square

In the non harmonic case, if the junctions are set such that $l_j = p_j/q_j$, where p_j and q_j are integers, prime with each other, then γ_{max} is periodic with period H_p such that

$$(4.4) \quad H_p = 2\pi \frac{LCM(q_1, \dots, q_{n-1})}{HCF(p_1, \dots, p_{n-1})},$$

see Fig. 4.1, where LCM is the Lowest Common Multiple and HCF the Highest Common Factor. To prove this write $f(x) = p(x - a_1)$ and use again the previous argument. In Fig. 4.1 we show the $\gamma_{max}(H)$ curve for a three junction unit such that $l_1 = 3/2$ and $l_2 = 5/3$ so that the period of $\gamma_{max}(H)$ is $H_p = 2\pi LCM(2, 3)/HCF(3, 5) = 12\pi$. In the following plots we will only show one period of $\gamma_{max}(H)$.

In the general case, we only have an approximate periodicity of $\gamma_{max}(H)$ which can be estimated using (4.4). Also, real junctions have a finite size which causes $\gamma_{max}(H) \rightarrow 0$, when $H \rightarrow +\infty$. Our model is thus valid as long as the dimensionless magnetic field H is not larger than $1/w_j$.

4.2. Influence of the position of the junction unit. In this section, we examine how the position of the set of junctions in the microstrip (linear domain) will affect the $\gamma_{max}(H)$ curve. For an array of junctions placed at the distances $\{a_i, i = 1, n\}$, we define a junction unit as the set $\{l_i, i = 1, n - 1\}$. Then the array where the junctions are at $\{a_1 + c, a_2 + c, \dots, a_n + c\}$ is the same junction unit. We define a_1 as the position of the junction unit. The length of the junction unit is $l_b = a_n - a_1$. The array is centered if $(a_n + a_1)/2 = l/2$.

Inline current feed: ($\nu = 0$)

Then the boundary conditions at the edge of the junction unit are $\phi'(a_1^-) = \phi'(0) = H - \gamma/2$, and $\phi'(a_n^+) = \phi'(l) = H + \gamma/2$, independently of the position of the junction unit.

PROPOSITION 4.2 (Inline junction unit). *For inline current feed, $\gamma_{max}(H)$ is independent of a_1 (the position of the junction unit) and of the length l of the cavity.*

Proof. Let $\phi_1(x)$ be a solution of (4.1), for given γ, H . Let us change the position of the junction unit to $a_1 + c$ so that the junctions are now placed at $\{a_1 + c, a_2 + c, \dots, a_n + c\}$. It is easy to see that $\phi_2(x) = \phi_1(x - c)$ satisfies the boundary conditions and is a solution. This one to one map between ϕ_1 and ϕ_2 exists for all c, H and γ so the two junction units have the same $\gamma_{max}(H)$. \square

Then the $\gamma_{max}(H)$ curve is independent of the position of junction unit when $\nu = 0$. By the same argument, we can show that $\gamma_{max}(H)$ is independent of the length l of the circuit (see Fig. 4.3). This curve depends only on the junction unit.

General current feed: ($0 < \nu \leq 1$)

Then the boundary conditions at the edge of the junction unit are:

$$\phi'(a_1^-) = -\nu j a_1 + H + (1 - \nu)\gamma/2, \quad \phi'(a_n^+) = H - (1 - \nu)\gamma/2 + \nu j(l - a_n).$$

Contrary to the inline feed, we cannot shift the phase to find a solution when the junction unit has been shifted, because now the boundary conditions depend on the position of the junction unit. Consider the derivative ϕ' at the boundaries of the junction unit. We will compare the curves $\gamma_{max}(H)$ for a centered unit and for a non centered unit. For a centered unit, $a_n - a_1 = l/2$ so that

$$\phi'(a_1^-) - H = -(\phi'(a_n^+) - H),$$

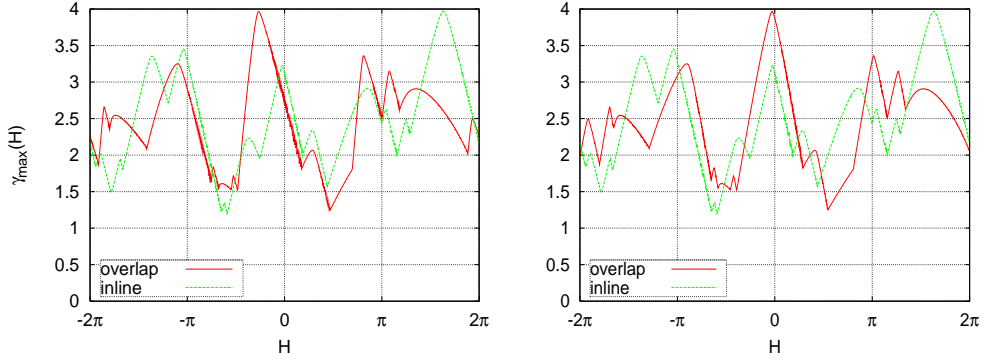


FIG. 4.2. Plot of $\gamma_{max}(H)$ for a four junctions device ($l = 10$, $d_i = 1$) such $l_1 = 1.5$, $l_2 = 2.5$, $l_3 = 2$. The left panel shows a non centered junction unit with $a_1 = 0.1$ and the right panel a centered unit with $a_1 = 2$. Notice the current dependent shift (4.5) for the overlap solution as one goes from a centered junction unit (right panel) to an off-centered junction unit (right panel). The junction unit was moved to the left.

but this equality is false for a non centered unit. It is possible to choose a correction H_ν to the magnetic field H in order to obtain the equality:

$$\begin{aligned}
 \phi'(a_1^-) - H + H_\nu &= -(\phi'(a_n^+) - H + H_\nu), \\
 -\nu j a_1 + (1 - \nu)\frac{\gamma}{2} + H_\nu &= -\left[\nu j(l - a_n) - (1 - \nu)\frac{\gamma}{2} + H_\nu\right], \\
 (4.5) \quad H_\nu &= \nu j \left(\frac{l_b - l}{2} + a_1\right).
 \end{aligned}$$

Let us consider two arrays, 1 with a centered junction unit and 2 with the same junction unit but non centered.

PROPOSITION 4.3 (Magnetic shift). *Let (H, γ_{max}) be the coordinates of a point of the $\gamma_{max}(H)$ curve for the circuit 1. Then $(H + H_\nu, \gamma_{max})$ is a point of the curve for the circuit 2.*

So, moving a junction unit translates the γ_{max} curve by $\nu j a_1$. Fig. 4.2 shows a $\gamma_{max}(H)$ for a four junctions device with a non centered junction unit in the left panel and a centered junction unit in the right panel. Both inline and overlap current feeds are presented. Notice the unchanged behavior for the inline current feed and the effect of $H_\nu (= -4.1\gamma/10)$ from (4.5) in the overlap case.

Proof. Let $\phi_{\{H, \gamma, b_1\}}$ be a solution for an array $A_1 \equiv \{a_1, \dots, a_n\}$ with a centered junction unit with γ and H given. Consider another array A_2 with the same junction unit moved by s , $A_2 \equiv \{a_1 + s, \dots, a_n + s\} \equiv A_1 + s$, the coefficients d_1, \dots, d_n being equal for the two circuits. From the solution $\phi_{\{H, \gamma, b_1\}}$ for A_1 we can deduce a solution $\psi_{\{H+H_\nu, \gamma, b_1+s\}}$ for A_2 . From (4.5) we have:

$$\psi'_{\{H+H_\nu, \gamma, b_1+s\}}(a_1^- + s) = \phi'_{\{H, \gamma, b_1\}}(a_1^-)$$

Taking,

$$\psi_{\{H+H_\nu, \gamma, b_1+s\}}(a_1^- + s) = \phi_{\{H, \gamma, b_1\}}(a_1^-)$$

and from the unicity of the solution, we obtain $\phi \equiv \psi$ in the two junction units. Thus, if ϕ is a solution for $\{H, \gamma\}$ given for A_1 , then ψ is a solution for $\{H + H_\nu, \gamma\}$ for A_2 , and vice versa.

Let $\gamma_{max,1}$ and $\gamma_{max,2}$ be the γ_{max} curves for the arrays A_1 and A_2 . From the solutions obtained for A_1 we build solutions for A_2 . As a consequence, $\gamma_{max,1}(H + H_\nu) \leq \gamma_{max,2}(H)$. On the other side, from solutions of A_2 we build solutions for A_1 , then $\gamma_{max,1}(H + H_\nu) \geq \gamma_{max,2}(H)$. So, we obtain the equality:

$$\gamma_{max,1}(H + H_\nu) = \gamma_{max,2}(H) .$$

□

Notice that this equality is independent of the number of junctions.

4.3. Comparison between inline and overlap current feeds. We now compare the γ_{max} curves for inline and overlap current feed. For one junction, the problem can be solved exactly using polynomials by parts (see remark 3.1). We obtain, $\gamma_{max}(H) = d_1$, for all ν . For two junctions there is the possibility of $d_1 \neq d_2$ and this will change $\gamma_{max}(H)$ qualitatively. Let us study the phase difference between two junctions. We use remark 3.1 and the boundary conditions to get

$$(4.6) \quad \begin{aligned} \phi_2 - \phi_1 &= -\frac{\nu j}{2}(a_2 - a_1)^2 + (P'(a_1) + d_1 \sin(\phi_1))(a_2 - a_1) , \\ \frac{\phi_2 - \phi_1}{a_2 - a_1} &= -\nu j \frac{a_2 + a_1}{2} + H - \frac{1 - \nu}{2}\gamma + d_1 \sin(\phi_1) . \end{aligned}$$

If $(a_2 + a_1)/2 = l/2$ (the junction unit is also centered), as $\gamma = jl$, (4.6) becomes:

$$(4.7) \quad \frac{\phi_2 - \phi_1}{a_2 - a_1} = H - \frac{\gamma}{2} + d_1 \sin(\phi_1) .$$

Note that we can obtain (4.7) from (4.6) with $\nu = 0$. We have shown that,

PROPOSITION 4.4 (Equivalence of all current feeds for a centered SQUID.). *For a centered two junctions device, all current feeds give the same γ_{max} curve.*

For an inline current feed, $\nu = 0$ so that the phase difference $\phi_2 - \phi_1$ is independent of the position of the junction unit. This is not true for the overlap feed, where moving the junction unit causes a "magnetic shift" as seen above in H_ν equation (4.5). When the number of the junctions $n \geq 3$, the γ_{max} curve depends on ν . The effect of the moving the junction unit on the γ_{max} curve was shown above. So, we can reduce the study to a centered junction unit. In this case, we have $a_1 = (l - l_b)/2$, and

$$(4.8) \quad \begin{aligned} \phi'(a_1^-) &= \phi'(0) + \int_0^{a_1^-} -\nu \frac{\gamma}{l} dx, \\ &= H - (1 - \nu) \frac{\gamma}{2} - \nu \frac{\gamma}{2} + \frac{\nu l_b}{l} \frac{\gamma}{2} = H - \left(1 - \frac{\nu l_b}{l}\right) \frac{\gamma}{2}, \\ \phi'(a_n^+) &= H + \left(1 - \frac{\nu l_b}{l}\right) \frac{\gamma}{2}, \end{aligned}$$

with $l_b = a_n - a_1$. We can write $\nu j = (\nu l_b/l)(\gamma/l_b)$, and $\nu l_b/l = \mu$. So, equation (4.1) is equivalent to the system:

$$(4.9) \quad -\phi''(x) + \sum_{i=1}^n d_i \delta(x - a_i) \sin(\phi) = \mu \frac{\gamma}{l_b} ,$$

with,

$$\phi'(a_1^-) = H - (1 - \mu)\gamma/2, \quad \phi'(a_n^+) = H + (1 - \mu)\gamma/2.$$

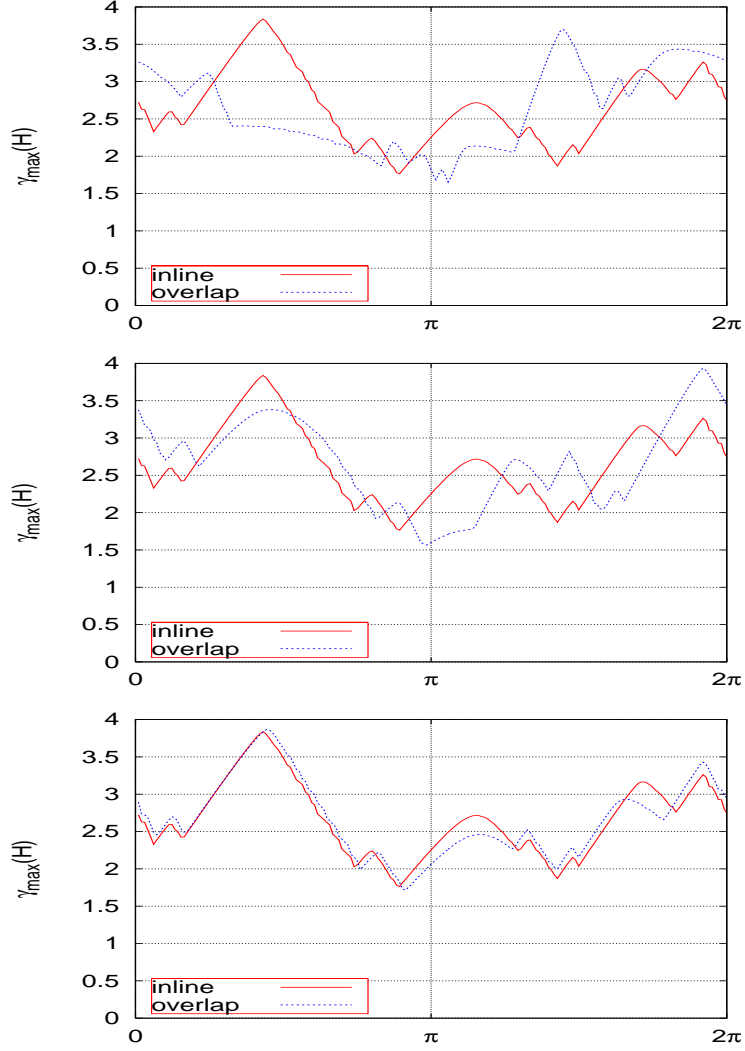


FIG. 4.3. Plot of $\gamma_{\max}(H)$ for the same centered junction unit $l_1 = 1, l_2 = 4, l_3 = 3, d_1 = d_2 = d_3 = d_4 = 1$ and different lengths l of the microstrip, from top to bottom $l = 8, 16$ and 64 . Notice how the overlap solution tends to the inline solution as one increases l .

As $0 \leq \nu \leq 1, 0 \leq \mu \leq l_b/l$. Note that l_b can be considered as the reference length of the device. Also note that if $l \rightarrow +\infty$ then $\mu \rightarrow 0$ and the equation (4.9) and boundary conditions tend to the situation of inline current feed. Fig. 4.3, illustrates this convergence when we increase the microstrip length l for a centered junction unit. Notice that the solution for the inline feed is not modified by the variation of length. With $l = 8$, we have a maximum difference between the solutions for the overlap and inline current feeds. As l increases the solution for overlap current feed tend to the solution for inline current feed. We prove this in the appendix 'Convergence of the solution for a large length l '.

Conclusion: In the appendix, we show that when $\nu\gamma/l$ tends to 0 the solution tends to the one for inline current feed. We can get this by increasing the length l or shrinking the junction area. (see in appendix 'Convergence by the coefficient d_i .'). We have three parameters: ν , l and γ_{max} . l is determined by the circuit. ν comes from the $2D$ model, it depends on the width of circuit. The third parameter, can be bounded from above: $0 \leq \gamma \leq \sum_i d_i$. We will see in the next section, what is the limit of $\gamma_{max}(H)$ for inline and overlap feeds when d_i are small.

4.4. The relation between inline and magnetic approximation. The size of the junctions $w_i < 1 < w$ so that $d_i \ll 1$ therefore the jump of the gradient of the phase across the junctions can be neglected. This is the magnetic approximation where only H fixes the phase gradient. In the previous section, we have shown that the solution for inline and overlap current feeds converge to the same $\gamma_{max}(H)$ curve for small d_i . We will show that this limit is the magnetic approximation.

Since $[\phi']_{a_i^-}^{a_i^+} = d_i \sin(\phi_i)$ (remark 3.2) and $j \leq \sum_i d_i/l$, then for small d_i , then ϕ tends to the linear function $\phi(x) = Hx + c$. This magnetic approximation seems crude but we show that it approaches the solution for inline feed, see the appendix "Inline - magnetic convergence". There we bound the difference between the γ curves for the inline feed and the magnetic approximation. Fig. 4.4 illustrates this convergence as d_i decreases.

This approximation gives very good results because we work on very small junctions and the corresponding $d_i \approx 10^{-2}$ (compared with the values taken in Fig. 4.4).

4.5. Magnetic approximation. The magnetic approximation is very interesting because it gives an analytic expression of $\gamma_{max}(H)$ and is independent of the value of the current and of the scale of the circuit. Here we consider that $\phi(x) = Hx + c$ and from (3.3)

$$\gamma = \sum_{i=1}^n d_i \sin(Ha_i + c) .$$

Notice that c is the only parameter which can be adjusted to reach the maximum.

To find the $\gamma_{max}(H)$ curve of the magnetic approximation, we take the derivative

$$(4.10) \quad \frac{\partial \gamma}{\partial c} = -\sin(c) \left(\sum_{i=1}^n d_i \sin(Ha_i) \right) + \cos(c) \left(\sum_{i=1}^n d_i \cos(Ha_i) \right) .$$

The values of c canceling $\partial\gamma/\partial c$ are

$$(4.11) \quad c_{max}(H) = \arctan \left(\frac{\sum_{i=1}^n d_i \cos(Ha_i)}{\sum_{i=1}^n d_i \sin(Ha_i)} \right) ,$$

and using (4.10), we have the solution:

$$(4.12) \quad \gamma_{max}(H) = \left| \sum_{i=1}^n d_i \sin(Ha_i + c_{max}(H)) \right| .$$

This γ_{max} curve is a function of H . A similar expression was given by Miller et al [10] for homogeneous arrays. Here we generalize this approach to nonhomogeneous arrays and justify it rigorously.

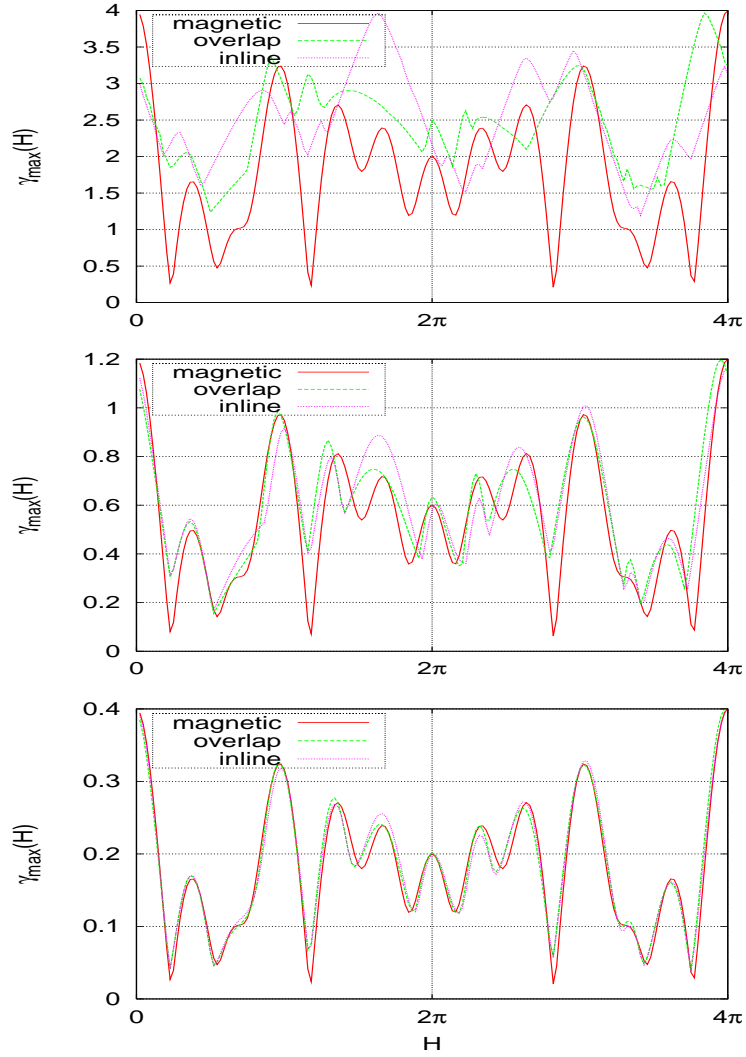


FIG. 4.4. Plot of $\gamma_{max}(H)$ for the same junction unit and different coefficients d_i which are all equal, from top to bottom $d_i = 1, 0.3$ and 0.1 . The distances between the junctions are $l_1 = 1.5$, $l_2 = 2.5$, $l_3 = 2$, $l = 10$.

Remark:

If $d_i = d, \forall i \in \{1, \dots, n\}$, we can simplify:

$$c_{max} = \arctan \left(\frac{\sum_{i=1}^n \cos(Ha_i)}{\sum_{i=1}^n \sin(Ha_i)} \right)$$

In the same way,

$$\gamma_{max} = d \left| \cos(c_{max}) \left(\sum_{i=1}^n \sin(Ha_i) \right) + \sin(c_{max}) \left(\sum_{i=1}^n \cos(Ha_i) \right) \right|.$$

Here changing the value of d will change linearly the amplitude of γ_{max} curve, this is not the case for the solutions of the boundary value problem (2.6). We can notice too, that the $\gamma_{max}(H)$ obtained from this approximation is invariant by the transformation,

$$\forall t \in \mathfrak{R}, \begin{cases} a_i & \rightarrow ta_i \\ H & \rightarrow \frac{1}{t}H \end{cases}.$$

We will show in the next sections that when $d_i \ll 1$, (4.12) provides a good estimate of the $\gamma_{max}(H)$ curve of a circuit. In addition, from its invariant properties we can compare different models and estimate the parameters of the circuit. It is a good approximation for the physical device. A cooperation has begun with the LERMA at the Observatoire de Paris to match theory and design for this type of circuit with specific properties[15].

5. Numerical solutions. We used two different methods, a stepping in the (H, γ) plane using a Newton iteration and what we call the method of implicit curves to find the maximal current of Eq.(4.1) for H given.

5.1. Newton's method. We start from the system of nonlinear transcendental equations (3.11) which is written for $n = 5$. Introducing the vector $X = (\phi_1, \phi_2, \dots, \phi_n)$, (3.11) can be written as $F(X) = 0$ where F is a nonlinear map from R^n to R^n . To solve numerically this equation, we use the Newton method.

$$X_{k+1} = X_k - (\nabla F(X_k))^{-1} F(X_k),$$

where $\nabla F(X_k)$ is the gradient of F evaluated at $X = X_k$. A first problem is to choose the initial vector X_0 . For that consider $H = 0$, there we expect a solution such that $\gamma \approx \sum_i^n d_i$ consequently $\phi_i \approx \pi/2 [2\pi]$. We have our initial vector. After finding the solution, we step in H and take as initial guess, the previous solution found, which for a small step in magnetic field is assumed to be close to the one we are looking for. By this way, we obtain a solution with a magnetic field $H + dH$ and a current γ . We can then increase γ until the method does not converge and this gives the maximum current $\gamma_{max}(H + dH)$ for increasing H . Similarly we can compute $\gamma_{max}(H)$ by starting with a large magnetic field and decrease H to 0. This curve will in general be different from the one obtained when increasing H due to hysteresis. The two curves need to be overlapped to see where is $\gamma_{max}(H)$. So, we introduce another method to be sure to obtain directly γ_{max} curve.

5.2. Implicit curves method. The polynomials (3.4) and (3.6) establish the existence and value of ϕ at the junctions. This function should satisfy the boundary conditions. The first one

$$\phi'(0) = P_1'(0) = H - (1 - \nu)\gamma/2$$

is true by construction, the second (for n junction circuit) is:

$$(5.1) \quad P_{n+1}'(l) = H + (1 - \nu)\frac{\gamma}{2},$$

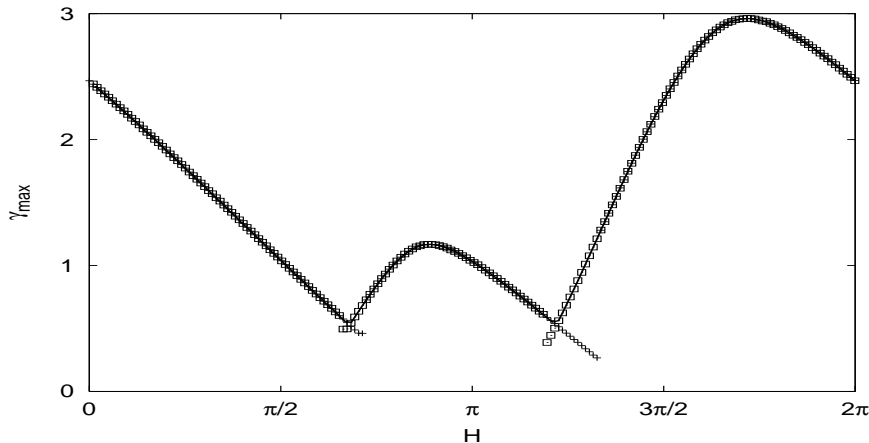


FIG. 5.1. Comparison between the Newton method and the implicit curve method for the γ_{max} curve for a three junction unit $a_1 = 1$, $a_2 = 2$, $a_3 = 3$, $d_1 = d_2 = d_3 = 1$, $\nu = 1$ and $l = 10$. The squares (resp. the +) symbols correspond to the Newton results for decreasing (resp. increasing) H and the continuous line corresponds to the results of the implicit curve method.

is true only for the solutions of Eq.(4.1). As we have remarked in the section "Polynomial by part", ϕ is entirely determined by ϕ_1 , γ and H . For H given, the solutions of Eq.(5.1) define a relation between ϕ_1 and γ . So, the maximal current solution depends on ϕ_1 and γ and Eq.(5.1) is the constraint it should satisfy. As the solutions ϕ are defined modulo 2π , see (3.1), we can assume $\phi_1 \in [-\pi, \pi]$. On the other hand, because of (3.3), $\gamma \in [0, \sum_i d_i]$. To solve this problem with Maple[16], we plot the implicit function (the constraint) of the two variables ϕ_1 and γ with H and ν fixed, defined by

$$(5.2) \quad P'_{n+1}|_{x=l}(\phi_1, \gamma, \nu, H) - H - \frac{1-\nu}{2}\gamma = 0,$$

with $(\phi_1, \gamma) \in [-\pi, \pi] \times [0, \sum_i d_i]$. The program searches, in an exhaustive way, the biggest value of γ of this implicit curve. Incrementing H , we obtain the relation $\gamma_{max}(H)$. We give an expression of P'_{n+1} for two and three junctions, in the Appendix: 'Implicit curves'.

Compared to the Newton method detailed in the previous section, this method has the advantage to converge to a global maximum γ_{max} , as long as we give enough points to plot the implicit curve. Fig. 5.1 compares $\gamma_{max}(H)$ using the two methods for a three junction unit. The solution given by the implicit curve method is in continuous line and superposes exactly with the other two plots. With the Newton method we can get trapped in local maxima while the implicit curve method always gives the global maximum. On the other hand the Newton method is much faster.

6. Two junctions. We have seen two methods to solve the problem numerically and established general properties. Now let us use these results for an array with a few junctions.

6.1. Same junction strength ($d = d_1 = d_2$). In Fig. 6.1, we plot in the left panel $\gamma_{max}(H)$ of a two junction unit. We find the expected periodicity $H_p = 2\pi/(a_2 - a_1)$, with a maximum for $H = 0$ in the inline case ($\nu = 0$). For the overlap feed, we have exactly the inline curve plus a magnetic shift. Notice that for the

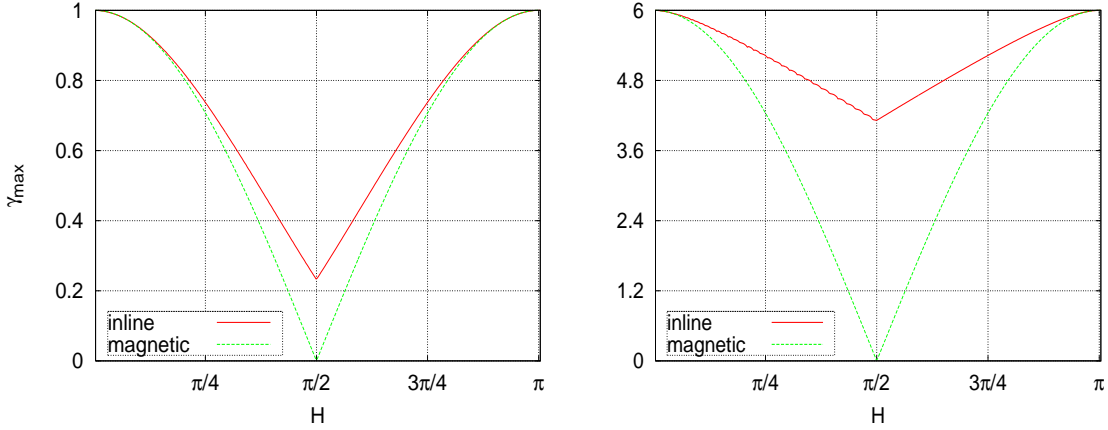


FIG. 6.1. Plot of the γ_{max} curve for a two junction unit such that $l_1 = 2$. In the left panel, $d_1 = d_2 = 0.5$ while on the right panel $d_1 = d_2 = 3$.

inline feed the amplitude of the γ_{max} curve is not proportional to d_i , contrary to the magnetic approximation. The larger the d_i the further away the $\gamma_{max}(H)$ curves are from the ones given by the magnetic approximation. This is expected because the magnetic approximation neglects the effect of d_i on the phase. In this section, to simplify the discussion we will restrict ourselves to the inline current feed. However the results will be valid for the general case. The maximum of γ_{max} corresponding to $H = 0 \text{ mod. } H_p$ is the only case where $(\phi_2 - \phi_1)/(a_2 - a_1) = H$. On the other hand, by construction, in the magnetic approximation $(\phi_2 - \phi_1)/(a_2 - a_1) = H$ for all H . In the general case, the closer H is to $\pi/(a_2 - a_1)$, the further $(\phi_2 - \phi_1)/(a_2 - a_1)$ is from H . This can be seen in the right panel of Fig. 6.2. So, there will be more tunneling current in one junction than in the other. This phenomenon increases as H increases from 0 to $\pi/(a_2 - a_1)$. For that value, we have two possible solutions for γ_{max} as shown in the left panel of Fig. 6.2 for $H = \pi/2$.

As the field crosses $\pi/(a_2 - a_1)$ the two junctions behave in opposite fashion as shown by the switch of the jumps in ϕ_x at the junctions, see right panel of Fig. 6.2. These two solutions or reversing behavior of junction, cause a jump in $\gamma'_{max}(H)$. As long as the evolution of ϕ_1 (or ϕ_2) is continuous there is no jump in γ'_{max} . To summarize, the smaller d is, the closer $(\phi_2 - \phi_1)/(a_2 - a_1)$ is to H . Another way of relaxing this constraint on $(\phi_2 - \phi_1)/(a_2 - a_1)$ for a constant d , is to separate the junctions and we can show that $l_b = a_2 - a_1 \rightarrow +\infty$ then $\gamma_{max}(H) \rightarrow d_1 + d_2$.

6.2. Regularity of $\gamma_{max}(H)$. Junctions are never perfectly similar, small differences in their areas or their critical currents will affect γ_{max} . In the left panel of Fig. 6.3 showing $\gamma_{max}(H)$ for a two junction device there is no discontinuity of the slope of the curve $\gamma_{max}(H)$ labeled "non equal", $\partial\gamma_{max}/\partial H$ exists everywhere. In this case, the value of $\phi_1(H)$ and $\phi_2(H)$ associated to $\gamma_{max}(H)$ vary continuously.

To show this, consider a circuit such that $d_1 > d_2$. Fixing $\phi_1 = \pi/2$, implies that $d_1 - d_2 \leq \gamma$ and consequently $d_1 - d_2 \leq \gamma_{max}$. From remark (3.3) we have $\gamma_{max} \leq d_1 + d_2$. Combining these inequalities we get $d_1 - d_2 \leq \gamma_{max} \leq d_1 + d_2$. Now let us find the values of H for which these bounds can be reached. From remark (3.3)

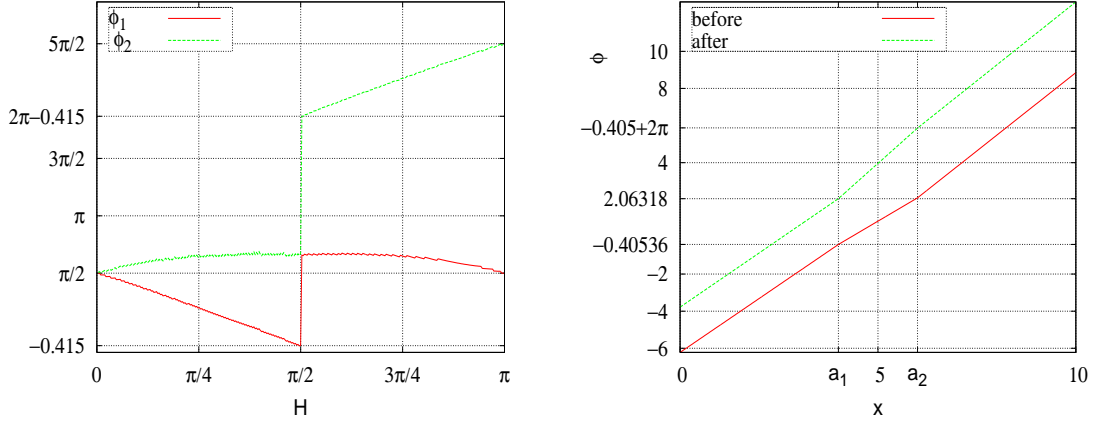


FIG. 6.2. *Left panel: plot of the phases ϕ_1 and ϕ_2 as a function of the magnetic field H for the same junction unit as the one shown in the left panel of Fig. 6.1 On the right panel, we plot $\phi(x)$ for the same device for $H < \pi/(a_2 - a_1)$ (continuous line) and $H > \pi/(a_2 - a_1)$ (dashed line).*

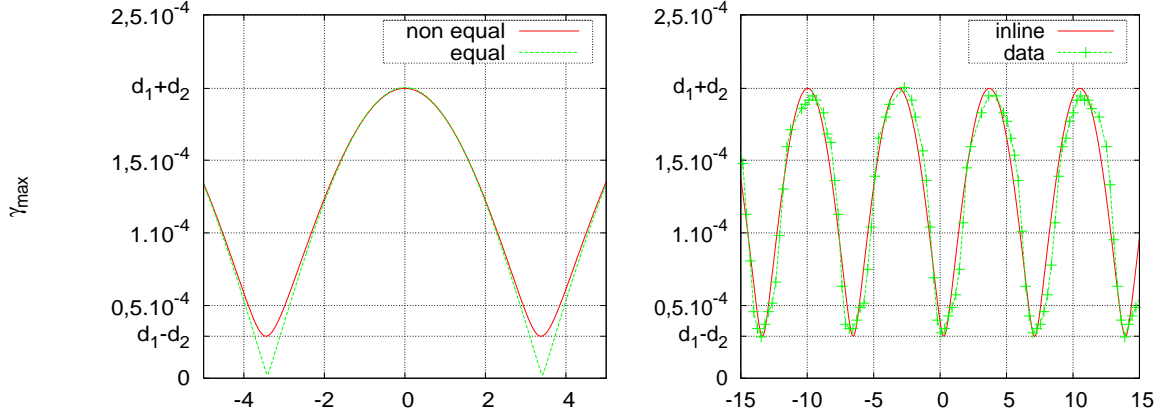


FIG. 6.3. *Plot of $\gamma_{max}(H)$ curves for two two junction units with inline current feed. On the left panel we compare $\gamma_{max}(H)$ given by the model for the cases $d_1 = d_2$ and $d_1 \neq d_2$. The right panel shows the fit of the experimental data from a two junction unit of the Observatory of Paris (Reproduced with permission of Faouzi Boussaha and Morvan Salez).*

and equation (3.6) we have

$$(6.1) \quad \begin{aligned} \gamma &= d_1 \sin(\phi_1) + d_2 \sin(\phi_2) , \\ \phi_2 &= -\frac{\nu j}{2} l_1^2 + \left(H - \left(\nu a_1 + \frac{1-\nu}{2} l \right) j + d_1 \sin \phi_1 \right) l_1 + \phi_1 , \end{aligned}$$

with $l_1 = a_2 - a_1$. By substituting the second equality into the first, and taking the derivative with respect to ϕ_1 , we obtain

$$\frac{\partial \gamma}{\partial \phi_1} = d_1 \cos \phi_1 + d_2 \left[\left(- \left(\nu \frac{a_2 + a_1}{2l} + \frac{1-\nu}{2} \right) \frac{\partial \gamma}{\partial \phi_1} + d_1 \cos \phi_1 \right) l_1 + 1 \right] \cos \phi_2 ,$$

Since we search for the maximum of γ , then $\partial\gamma/\partial\phi_1 = 0$, so that

$$(6.2) \quad d_1 \cos \phi_1 = -d_2 (d_1 l_1 \cos(\phi_1) + 1) \cos \phi_2 .$$

When $\phi_1 = \pi/2$, this condition gives $\phi_2 = \pi/2$ modulo π . Now, inserting these solutions in (6.1), we obtain the values of H for which these solutions are possible.

$\gamma_{max}(H)$	H
$d_1 + d_2$	$2k\pi/l_1 + [\nu(a_1 + l_1/2) + (1 - \nu)l/2](d_1 + d_2)/l - d_1$
$d_1 - d_2$	$(2k + 1)\pi/l_1 + [\nu(a_1 + l_1/2) + (1 - \nu)l/2](d_1 - d_2)/l - d_1$

This enables from the curve $\gamma_{max}(H)$ to estimate d_1 and d_2 .

We now proceed to give the condition between d_1 and d_2 such that the behavior of the γ_{max} relation changes. Since $\phi_2(H)$ varies continuously, $\cos(\phi_2)$ takes all the values between -1 and 1 . We assume that $\forall\phi_1, d_1 l_1 \cos(\phi_1) + 1 \geq 0$ where $l_1 = a_2 - a_1$ ¹. We consider two cases:

1. $\cos \phi_1 \leq 0$: as $\cos \phi_1 \geq -1$ from (6.2) we obtain,

$$d_2 \cos(\phi_2) \leq \frac{d_1}{1 - d_1 l_1} .$$

Since $\cos(\phi_2)$ must take all values between -1 and 1 and $d_2 > 0$

$$(6.3) \quad d_2 \leq \frac{d_1}{1 - d_1 l_1} .$$

This is the maximal value than d_2 can take compared to d_1 .

2. $\cos \phi_1 \geq 0$: as $\cos \phi_1 \leq 1$, for the same reason we obtain:

$$(6.4) \quad d_2 \geq \frac{d_1}{1 + d_1 l_1} .$$

To summarize $d\gamma_{max}(H)/dH$ does not vary continuously if

$$(6.5) \quad \frac{d_1}{1 - d_1 l_1} \leq d_2 \leq \frac{d_1}{1 + d_1 l_1} .$$

To illustrate this effect we consider the configuration of a a microstrip with inline current feed with two Josephson junctions built by Morvan Salez and Faouzi Boussaha at the Observatoire de Paris. The results are shown in Fig. 6.3. The square junctions have an area of $w_j^2 \approx 1\mu m^2$, the Josephson length is $\lambda_J = 5.6\mu m$ and $l_1 = a_2 - a_1 = 13\mu m$ (using the junction centers). This gives $d_1 = d_2 \approx 0.0357$, $l_1 \approx 2.32$ if the areas are equal. However the experimental data does not go to 0 so that the junctions are probably slightly different as expected from (6.3) and (6.4),

$$0.032969 \leq d_2 \leq 0.038923 .$$

Only a 10% difference in area is enough to give a regular $\gamma_{max}(H)$. From the fit of the experimental data (right panel of Fig. 6.3) we can estimate the areas of the junctions as $w_1^2 = 0.85255\mu m^2$ and $w_2^2 = 1.1417\mu m^2$.

As we have seen in the previous section, when the γ_{max} curve does not show any spike, it is bounded by $d_1 + d_2$ and $|d_1 - d_2|$. From this we can obtain the characteristics of the two junctions, their critical current density and area except that we do not know which junction corresponds to d_1 and which to d_2 . However if the γ_{max} does not have any spikes then we can give the exact area of the junctions assuming the critical density current is known.

¹for small junctions this is not a strong constraint, because since $d_i = w_i^2/w \ll 1$, w_i , $w \ll 1$ and $l_i \ll 1$ are about 10^{-2} .

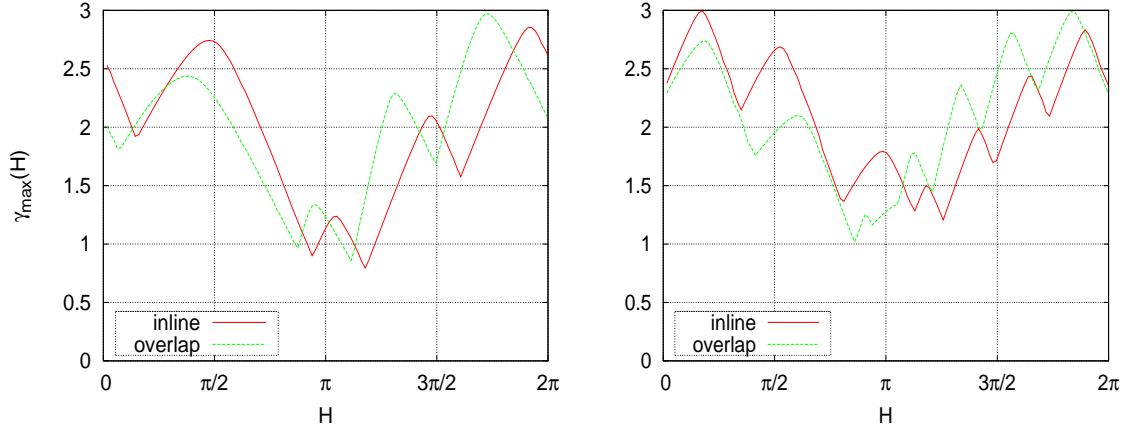


FIG. 7.1. Plot of $\gamma_{max}(H)$ curves for a two junction unit $a_1 = 1$, $a_2 = 2$ ($l_1 = 1$) and a third junction placed at $a_3 = 5$, $l_2 = 3$ (left panel) and $a_3 = 8$, $l_2 = 6$ (right panel). All the junctions have the coefficient $d_i = 1$.

7. Many junctions. A two junctions circuit is a SQUID and shows a simple $\gamma_{max}(H)$. To obtain specific properties for advanced detectors, experimentalists make devices with more junctions.

7.1. 3 Josephson junctions. When we add a new junction to a circuit with two junctions, new oscillations appear on $\gamma_{max}(H)$. We cannot predict the amplitude of the oscillations but from l_1 and l_2 we can estimate the number of oscillations in one period i.e. the interval $[0, H_p]$. We introduce the phase difference for $H = 0$, $\Delta\phi_i \equiv \phi_i - \phi_1$. Using Proposition 4.1, we can state that as H goes from 0 to H_p , $\phi_2 - \phi_1$ goes from $\Delta\phi_2$ to $\Delta\phi_2 + 2\pi l_1/l_1 = \Delta\phi_2 + 2\pi$. Similarly $\phi_3 - \phi_1$ goes from $\Delta\phi_3$ to $\Delta\phi_3 + 2\pi(l_2 + l_1)/l_1 = \Delta\phi_3 + 2\pi(l_2/l_1 + 1)$ which becomes $\Delta\phi_3 + 2\pi(k + 1)$ if the junctions are placed harmonically so that $l_2 = kl_1$. In that case we expect the $\gamma_{max}(H)$ curve to present $k + 1$ bumps within one period. In Fig. 7.1, the junctions are placed in a harmonic way $a_3 - a_2 = k(a_2 - a_1)$, where $k = 3$ (left panel) and $k = 6$ (right panel). As expected we see the 4 intermediate "bumps" in the $\gamma_{max}(H)$ curve in the left panel and 7 "bumps" in the curve of the right panel. We can see the periodicity given by $H_p = 2\pi/(a_2 - a_1) \equiv 2\pi/l_1$, which adds new oscillations. This picture shows that the closer the third junction is to the junction unit the fewer oscillations there are. Then the oscillations have a larger amplitude. These estimations hold approximately in the case of an array with more junctions.

In other words, when $a_3 - a_1$ is large as in the right panel of Fig. 7.1 and the left panel of Fig. 7.2, the shape of γ_{max} curve tends to the one for a two junctions circuit. We explain this below.

7.2. Influence of a faraway single junction for the inline current feed. In Fig. 7.2, for each panel, we plot a γ_{max} curve, for a n junction unit, and another with the same junction unit plus a far away junction. The γ_{max} curve for $n + 1$ junctions look like n junctions curves to which a shift has been added. Let us evaluate this shift.

Remark that for the junction n , using the notations of Eq. (3.4) and (3.6), we know that ϕ_{n+1} is determined by P_{n+1} . If we increase P'_{n+1} of ϵ , then ϕ_{n+1} increase of $\epsilon(a_{n+1} - a_n)$. Thus, a variation at ϕ_n of $\epsilon = \pm\pi/(a_{n+1} - a_n)$ is enough to obtain

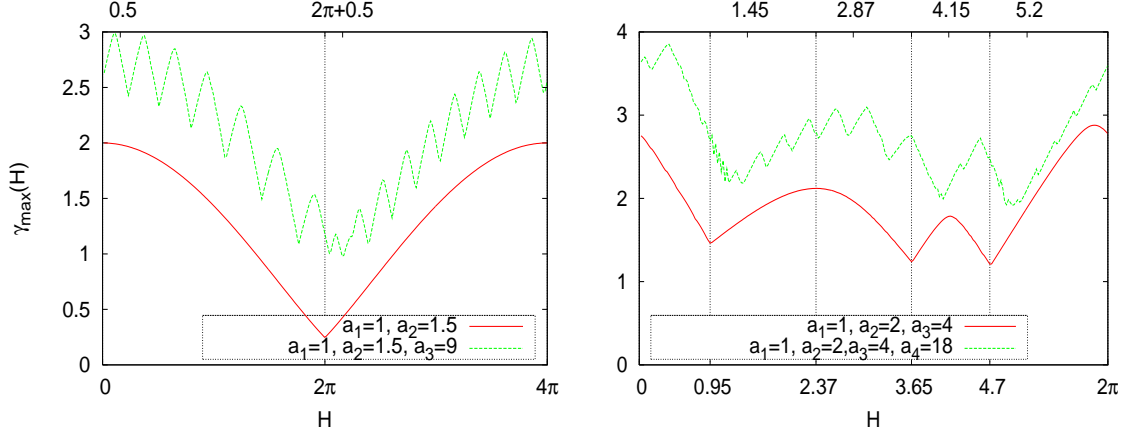


FIG. 7.2. Plot of $\gamma_{max}(H)$ showing the influence of a far away junction on a junction unit. In continuous line we plot $\gamma_{max}(H)$ for the junction unit only and in dashed line we plot $\gamma_{max}(H)$ for the junction unit together with the far away junction. The left panel shows a two junction unit together with a third junction and the right panel a three junction unit together with a four junction. The H scale on the bottom of the graphs indicates local minima or maxima of the junction unit curves and the scale at the top shows these locations shifted by the quantity (7.1). the continuous line corresponds to the junction unit only For all devices $d_i = 1$.

$\sin \phi_{n+1} = 1$. The farther the last junction, the smaller ϵ , and consequently this junction has the smallest action on the junction unit. So, in the search of γ_{max} , the value of $\sin \phi_{n+1}$ is near 1. The γ_{max}^{n+1} curve of a circuit with $n + 1$ junctions is close to $\gamma_{max}^n + d_{n+1}$ i.e. the curve for the n junction circuit with n junctions plus the maximal contribution of the last junction.

Now let us assume that $\sin \phi_{n+1} = 1$. Let us recall the boundary conditions of our inline current feed problem: $\phi'|_{\{0,l\}} = H \mp \gamma/2$. Therefore the boundary conditions at the junction unit are $\phi'(0) = H - \gamma/2$ and for x such that $a_n < x < a_{n+1}$, $\phi'(x) = H + \gamma/2 - d_{n+1}$. As we have done in the section "magnetic shift", let $H' = H - d_{n+1}/2$. The previous boundary conditions become

$$\phi'|_{\{0,a_n^+\}} = H' \mp \frac{\gamma}{2}.$$

We find the desired boundary values. Finally we obtain:

$$(7.1) \quad \lim_{a_{n+1}-a_n \rightarrow +\infty} \gamma_{max}^{n+1} \left(H + \frac{d_{n+1}}{2} \right) = \gamma_{max}^n(H) + d_{n+1}$$

Fig. 7.2 illustrates this convergence.

This argument can not be extended simply to the overlap or general current feed for two reasons. First introducing or taking out the last junction a_{n+1} induces a variation of the magnetic shift H_ν given by (4.5). We could estimate it but we have the problem that the curvature of ϕ , for n junctions device is $\nu j/2$ where j depends on the number of the junctions. This will affect the shift between the junctions and consequently the curve γ_{max} .

However, numerical simulation show that Eq. (7.1) remains a good approximation for the general case (same order from inline) even with a small number of junctions. The general feed and inline feed problems coincide when $d_{n+1}/\sum_1^n d_i$ tends to zero.

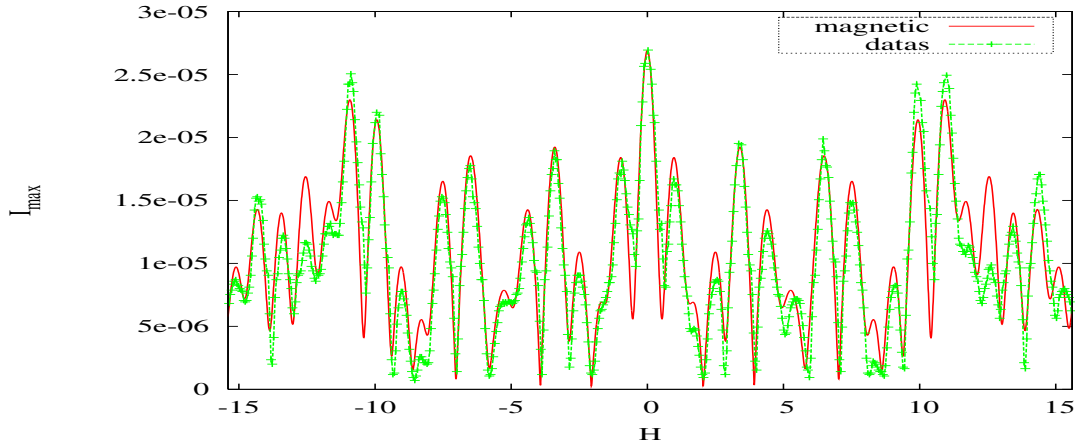


FIG. 7.3. Experimental $I_{\max}(H)$ for an array of five junctions in a 2D microstrip line built by M. Salez and F. Boussaha of the Observatory of Paris (Reproduced with their permission). The measured data is presented by the + symbols and the magnetic approximation result is in continuous line.

Going back to the physical device, this means that the forces of the junctions are very small $d_i \approx 10^{-2}$ and for these values the inline and overlap results are practically indiscernible from the magnetic approximation. Then (7.1) can be used.

7.3. A real device with 5 Josephson junctions. We have compared our theory to the experimental results for a device with two Josephson junctions. The same team at the Observatoire de Paris, has made a device with five junctions. Here the γ_{\max} curve obtained is totally different from the one for a simple SQUID. The parameters are $l_1 = 20$, $l_2 = 42$, $l_3 = 12$ and $l_4 = 6$. Fig. 7.3 shows the γ_{\max} curve where the current and magnetic field have been scaled using approximately the same factors as for the SQUID of Fig. 6.2. Our modeling approach also gives excellent agreement for experimental uniform arrays of 5, 10 and 20 junctions.

8. Conclusion. We have analyzed mathematically a new continuous/discrete model for describing arrays of small Josephson junctions. Compared to standard "lumped" approaches, we do not approximate the equations, except for neglecting the phase variation in the junction. In particular our approach preserves the matching at the interface.

We establish the periodicity of the $\gamma_{\max}(H)$ curve, show how it depends on the position of the array with respect to the microstrip. This is particularly interesting to estimate the proportion of inline current feed versus overlap feed. We show how separating a junction from an array will influence $\gamma_{\max}(H)$.

We introduce a numerical method for estimating $\gamma_{\max}(H)$ which is more reliable than the standard Newton method used up to now.

The relative simplicity of the model allows in depth analysis that is out of reach for the 2D model. In particular we show that solutions for general current feed tend to the solutions of inline feed when $\nu j/l \rightarrow 0$. All models reduce to what we call the magnetic approximation for small d_i .

Our global model gives a very good agreement with experimental curves obtained for arrays of up to five junctions. The simplicity of the magnetic approximation allows to address the Inverse problem of determining features of the array from $\gamma_{\max}(H)$.

Acknowledgements

J.G.C. and L. L. thank Faouzi Boussaha and Morvan Salez for helpful discussions and for their experimental results. The authors thank Yuri Gaididei for useful suggestions. The computations were done at the Centre de Ressources Informatiques de Haute-Normandie (CRIHAN).

REFERENCES

- [1] B. D. JOSEPHSON, *Phys. Lett.* **1**, 251, (1962).
- [2] A. BARONE AND G. PATERNO, *Physics and Applications of the Josephson effect*, J. Wiley, (1982).
- [3] K. LIKHAREV, *Dynamics of Josephson junctions and circuits*, Gordon and Breach, (1986).
- [4] M. SALEZ ET AL., Proc. SPIE Conf. on Telescopes and Astronomical Instrumentation, Hawaii, 2002 (August 22-28), col. 4855, p. 402, Proc. 4th European Conference on applied superconductivity, EUCAS 99, 651, (1999)
- [5] J. G. CAPUTO, N. FLYTZANIS AND M. VAVALIS, *A semi-linear elliptic pde model for the static solution of Josephson junctions*, International Journal of Modern Physics C, vol. 6, No. 2, 241-262, (1995).
- [6] J. G. CAPUTO, N. FLYTZANIS, Y. GAIDIDEI AND M. VAVALIS, *Two-dimensional effects in Josephson junctions: I static properties*, Phys. Rev. E, 54, No. 2, 2092-2101, (1996).
- [7] A. BENABDALLAH, J. G. CAPUTO AND N. FLYTZANIS, *The window Josephson junction: a coupled linear nonlinear system*, Physica D, 161, 79-101, (2002).
- [8] J. G. CAPUTO AND Y. GAIDIDEI, *Two point Josephson junctions in a superconducting stripline: static case.*, Physica C, 402, 160-173, (2004).
- [9] J. G. CAPUTO AND L. LOUKITCH, *Dynamics of point Josephson junctions in microstrip line.*, Physica **425** (2005) 69-89.
- [10] J. H. MILLER, JR., G. H. GUNARATNE, J. HUANG, AND T. D. GOLDING, *Appl. Phys. Lett.* 59, (25), 3330 (1991).
- [11] J. G. CAPUTO, N. FLYTZANIS, A. TERSENOV AND M. VAVALIS, *Analysis of a semi-linear pde for modeling static solutions of Josephson junctions*, SIAM J. of Math. Analysis, **34**, 1356-1379, (2003).
- [12] A. V. USTINOV, M. CIRILLO, B. H. LARSEN, V. A. OBOZNOV, P. CARELLI, AND G. ROTOLI, *Phys. Rev. B* 51, (5), 3081 (1995).
- [13] R. FEHRENBACHER, V. B. GESHKENBEIN AND G. BLATTER, *Pinning phenomena and critical currents in disordered long Josephson junctions*, Phys. Rev. B **45**, 5450, (1992).
- [14] M. A. ITZLER AND M. TINKHAM, *Flux pinning in large Josephson junctions with columnar defects*, Phys. Rev. B **51**, 435, (1995), *Vortex pinning by disordered columnar defects in large Josephson junctions*, Phys. Rev. B **53**, 11949, (1996)
- [15] M. SALEZ, F. BOUSSAHA, J. G. CAPUTO AND L. LOUKITCH, *SQUID properties of non-uniform, parallel superconducting junction arrays*, In press.
- [16] <http://www.maplesoft.com/>

9. Appendix.

9.1. Implicit curves. In this part, we give an example, of $P'_{n+1}(x)$ for systems with three junctions. We denote:

$$\begin{cases} \sin_1 &= \sin(\phi_1), \\ C_1 &= (d_1 \sin(\phi_1) - \frac{\nu\gamma a_1}{l} + H - (1 - \nu) \frac{\gamma}{2}) (a_2 - a_1) + \phi_1, \\ D_j &= \frac{\nu\gamma(a_{j+1} - a_j)^2}{2l}. \end{cases}$$

Then equations (3.4) and (3.6) give

$$(9.1) \quad P'_3(x) = -\frac{\nu\gamma x}{l} + d_2 \sin(-D_1 + C_1) + d_1 \sin_1 + H - (1 - \nu) \frac{\gamma}{2}.$$

$$\begin{aligned} P'_4(x) &= -\frac{\nu\gamma x}{l} + d_3 \sin \left[-D_2 + \left\{ -d_2 \sin(D_1 - C_1) - \frac{\nu\gamma a_2}{l} \right. \right. \\ &\quad \left. \left. + d_1 \sin_1 + H - (1 - \nu) \frac{\gamma}{2} \right\} (a_3 - a_2) - D_1 + C_1 \right] \end{aligned}$$

$$(9.2) \quad +d_2 \sin(-D_1 + C_1) + d_1 \sin_1 + H - (1 - \nu) \frac{\gamma}{2}.$$

This example shows that $P'_k(x)$ is C^∞ in the variables $(\gamma, \phi_1, \nu, H, x)$. In particular $P'_n(l)$ is C^∞ in the variables (γ, ϕ_1, ν, H) .

9.2. The current feed factor ν : analytical estimates. Equation (4.9) shows that we tend to an inline current feed when l is large. However we should show that the γ_{max} curve tends to the one for the inline feed.

LEMMA 9.1 (Solution). *For all ϕ_1 and H , there exists a γ such that equation (4.1) has a solution.*

Proof. As we have seen in the section "Implicit curves method", it is sufficient to solve equation (5.1): $P'_{n+1}(l) = H + (1 - \nu)\gamma/2$, to find a solution. Let us fix a value for ϕ_1 with ν, H, l given. If, $\gamma < -\sum_{i=1}^n d_i$, then $P'_{n+1}(l) < H + (1 - \nu)\gamma/2$. Conversely when $\gamma > \sum_{i=1}^n d_i$, we obtain $P'_{n+1}(l) > H + (1 - \nu)\gamma/2$. But by construction, $P'_{n+1}(l)$ is a function continuous in all its variables, in particular γ . Thus we have at least one value of γ in $[-\sum_{i=1}^n d_i, \sum_{i=1}^n d_i]$, such that $P'_{n+1}(l) = H + (1 - \nu)\gamma/2$ so that it is a solution for that value of ϕ_1 . \square

We want to study the variation of $\gamma(H)$ versus the current feed ν . At this point, we do not consider the γ_{max} curve. Let us fix ϕ_1 . Using the previous property, we know that there exists at least one solution of equation (4.1), and particularly almost one γ . Without changing ϕ_1 or H , we plot all the possible γ versus ν in Fig. 9.1. We call this curve $\gamma(\nu)$ curve. To plot this $\gamma(\nu)$ curve, we use the same parameter as in Fig. 4.3, with $H = 1.3617$ (see top panel, we choose this H because there is a big difference between the solution for inline and overlap current feeds). We choose for ϕ_1 the value found with Maple giving the maximum γ_{max} for the inline feed. Fig. 9.1, top panel, for $\nu = 0$, confirms the γ_{max} value found in Fig. 4.3. But for overlap the maximum current we can obtain is near 0. So, there is another value of ϕ_1 for γ_{max} of overlap current feed ($\phi_1 \approx 0.252$).

Let us study $\gamma(\nu)$ curve. By definition, $\gamma = \sum_{i=1}^n d_i \sin(\phi_i)$. Let ϕ_1 be a value such $\partial\gamma/\partial\nu$ exists, then:

$$(9.3) \quad \begin{aligned} \frac{\partial\gamma}{\partial\nu} &= \sum_{i=1}^n d_i \frac{\partial\phi_i}{\partial\nu} \cos(\phi_i), \\ \left| \frac{\partial\gamma}{\partial\nu} \right| &\leq \sum_{i=1}^n d_i \left| \frac{\partial\phi_i}{\partial\nu} \right|. \end{aligned}$$

With $\phi_i = \phi(a_i)$, and we note in the following $\phi'_i = \lim_{\epsilon \rightarrow 0} \phi'(a_i - \epsilon)$ (the left derivative of ϕ). Let us make some remarks: as ϕ_1 is fixed,

$$\begin{aligned} \left. \frac{\partial\phi_1}{\partial\nu} \right|_{\nu=0} &= 0 \\ \frac{\partial\phi'_1}{\partial\nu} &= \frac{\partial}{\partial\nu} \left\{ H - \left(\frac{1}{2} - \frac{\nu l_b}{2l} \right) \frac{\gamma}{2} \right\} = - \left(\frac{1}{2} - \frac{\nu l_b}{2l} \right) \frac{\partial\gamma}{\partial\nu} + \frac{l_b \gamma}{4l}, \end{aligned}$$

using (3.4) and (3.6) we can begin iteration,

$$\begin{aligned} \frac{\partial\phi_i}{\partial\nu} &= - \left(\nu \frac{\partial\gamma}{\partial\nu} + \gamma \right) \frac{l_{i-1}^2}{2l} + l_{i-1} \frac{\partial\phi'_{i-1}}{\partial\nu} + \frac{\partial\phi_{i-1}}{\partial\nu} (d_{i-1} l_{i-1} \cos(\phi_{i-1}) + 1), \\ \frac{\partial\phi'_i}{\partial\nu} &= - \left(\nu \frac{\partial\gamma}{\partial\nu} + \gamma \right) \frac{l_{i-1}}{l} + d_{i-1} \frac{\partial\phi_{i-1}}{\partial\nu} \cos(\phi_{i-1}) + \frac{\partial\phi'_{i-1}}{\partial\nu}, \end{aligned}$$

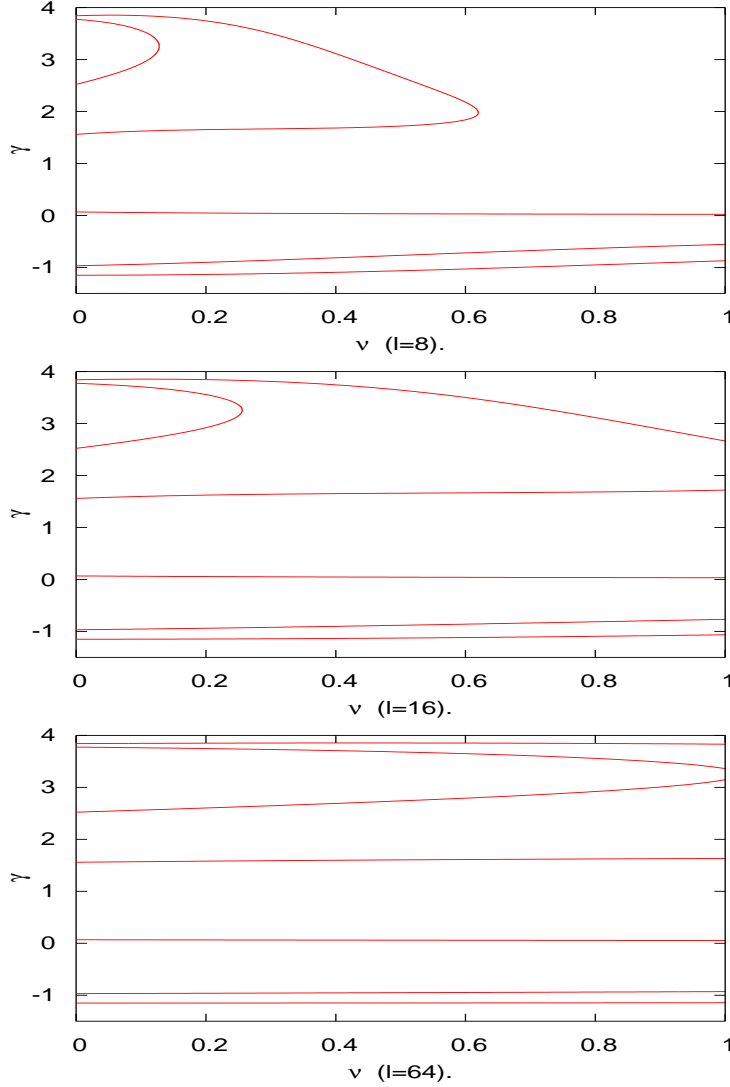


FIG. 9.1. Each panels corresponds to device of the panels of the Fig. 4.3. We plot the implicit curve $\gamma(\nu)$ curve for $H = 1.3617$, $\phi_1 = 1.3897$. This coordinates give the maximum of the $\gamma_{max}(H)$ of inline of the top panels of the Fig. 4.3. From top to bottom we increase the length of the device and we notice the stretching of the $\gamma(\nu)$ curve (with the coefficient found in equation (4.9): l_b/l).

with $l_i = a_{i+1} - a_i$. This last equation can be written, for $i \geq 3$:

$$\left. \frac{\partial \phi'_i}{\partial \nu} \right|_{\nu=0} = - \left(\nu \frac{\partial \gamma}{\partial \nu} + \gamma \right) \frac{a_i - a_1}{l} + \left. \frac{\partial \phi'_1}{\partial \nu} \right|_{\nu=0} + \sum_{k=2}^{i-1} d_k \frac{\partial \phi_k}{\partial \nu} \cos(\phi_k).$$

We obtain,

$$\frac{\partial \phi_{i+1}}{\partial \nu} = -K_1^i \frac{\partial \gamma}{\partial \nu} - K_2^i \gamma + \frac{\partial \phi_i}{\partial \nu} + l_i \sum_{k=2}^i d_k \frac{\partial \phi_k}{\partial \nu} \cos(\phi_k),$$

$$K_1^i = l_i \left[\frac{\nu l_i}{2l} + \nu \frac{a_{i+1} - a_1}{l} + \frac{1}{2} - \frac{\nu l_b}{2l} \right],$$

$$K_2^i = l_i \left[\frac{l_i}{2l} + \frac{a_{i+1} - a_1}{l} - \frac{l_b}{2l} \right].$$

Applying absolute values, we obtain:

$$(9.4) \quad \left| \frac{\partial \phi_{i+1}}{\partial \nu} \right| \leq K_1^i \left| \frac{\partial \gamma}{\partial \nu} \right| + K_2^i |\gamma| + \left| \frac{\partial \phi_i}{\partial \nu} \right| + l_i \sum_{k=2}^i d_k \left| \frac{\partial \phi_k}{\partial \nu} \right|,$$

We do not need to find exact expression of $|\partial \phi_{i+1}/\partial \nu|$, we know that it is a linear combination of $|\partial \gamma/\partial \nu|$ and $|\gamma|$ and so is $|\partial \phi_2/\partial \nu|$. Using (9.4), we can show by iteration that $|\partial \phi_i/\partial \nu|$ is a linear combination of $|\partial \gamma/\partial \nu|$ and $|\gamma|$. Applying this last remark to inequality (9.3), we obtain that there exists two constants, C_1 and C_2 such

$$\left| \frac{\partial \gamma}{\partial \nu} \right| \leq C_1 \left| \frac{\partial \gamma}{\partial \nu} \right| + C_2 |\gamma|,$$

C_1 and C_2 are combination of d_i , l_i , K_1^i and K_2^i . For ν and d_i sufficiently small $|C_1| < 1$, then

$$(9.5) \quad \left| \frac{\partial \gamma}{\partial \nu} \right| \leq \frac{C_2}{1 - C_1} |\gamma|.$$

This last equation implies local continuity of the γ curve as a function of ν . As we have seen in section "Comparison between inline and overlap" increasing l is equivalent to decreasing the range of ν (given by μ). $\forall \epsilon, \exists L/ l \geq L \Rightarrow \mu \leq \epsilon$. This shows the convergence of γ_{max} ($0 \leq \nu \leq 1$) curve to inline current feed when $l \rightarrow +\infty$.

9.3. Convergence by the junction coefficient d_i . We want to show that the general case convergence to inline case, for small d_i . We have shown in the axiom of the previous appendix that for H and ϕ_1 given, we can find almost one solution, whatever ν . This show that for the same ϕ_1 , we can find a general and an inline solution. Let us define:

1. $P_n^i(x), \forall x \in]a_n, a_{n+1}[$ a solution of inline problem ($\nu = 0$) of this circuit, γ^i the maximal current associated at the value ϕ_1 .
2. $P_n^g(x), \forall x \in]a_n, a_{n+1}[$ a general solution ($\nu \neq 0$, same l and same junction unit), γ^g the maximal current associated at the value ϕ_1 .
3. α_j and β_j by:
$$\begin{cases} \alpha_j &= P_j^{g'}(a_j) - P_j^{i'}(a_j), \\ \beta_j &= P_j^g(a_j) - P_j^i(a_j). \end{cases}$$

As $P_1^g(a_1) = \phi_1 = P_1^i(a_1)$, we have $\beta_1 = 0$. We can calculate α_1 using (4.8),

$$\alpha_1 = P_1^{g'}(a_1) - P_1^{i'}(a_1) = -\frac{\gamma^i - \gamma^g}{2} + \frac{\nu l_b}{2l} \gamma^g.$$

But γ^i and γ^g are positive, so

$$(9.6) \quad |\alpha_1| \leq \left(\frac{1}{2} + \frac{\nu l_b}{2l} \right) \sum_{i=1}^n d_i.$$

The aim of this following part is to bound β_i . We proceed by iteration. We recall that $l_k = a_{k+1} - a_k$. Using (3.6) we estimate β_{k+1} :

$$(9.7) \quad \beta_{k+1} = \frac{-\nu \gamma^g}{2l} l_k^2 + [d_k (\sin(P_k^g(a_k)) - \sin(P_k^i(a_k))) + \alpha_k] l_k + \beta_k.$$

Let us focus on the sine terms,

$$\begin{aligned}\sin(P_k^g(a_k)) - \sin(P_k^i(a_k)) &= \sin(P_k^i(a_k) + \beta_k) - \sin(P_k^i(a_k)), \\ &= \sin(P_k^i(a_k)) [\cos(\beta_k) - 1] + \sin(\beta_k) \cos(P_k^i(a_k)), \\ &\leq |\beta_k|^2 + |\beta_k|.\end{aligned}$$

We assume $\beta_k \ll 1$, thus we obtain the equivalences $\sin(\beta_k) \approx \beta_k$ and $\cos(\beta_k) - 1 \approx -\beta_k^2$, but we cannot predict the sign of $\sin(P_k^i(a_k))$ or $\cos(P_k^i(a_k))$. We neglect $|\beta_k|^2$ compared to β_k . From (9.7),

$$\begin{aligned}|\beta_{n+1}| &\leq \left| \frac{\nu\gamma^g}{2l} l_n^2 \right| + (d_n |\beta_n| + |\alpha_n|) l_n + |\beta_n|, \\ |\alpha_{n+1}| &\leq \left| \frac{\nu\gamma^g}{l} l_n \right| + d_n |\beta_n| + |\alpha_n|.\end{aligned}$$

Let us note $G = \nu \sum_{i=1}^n d_i/l$, we obtain a simple system

$$(9.8) \quad \zeta_{n+1} \leq M_n \zeta_n + G V_n ,$$

with, $\zeta_n = \begin{pmatrix} |\beta_n| \\ |\alpha_n| \end{pmatrix}$, $M_n = \begin{pmatrix} d_n l_n + 1 & l_n \\ d_n & 1 \end{pmatrix}$ and $V_n = \begin{pmatrix} l_n^2/2 \\ l_n \end{pmatrix}$. So, we bound $|\beta_n|$ and $|\alpha_n|$, with $|\beta_1|$ and $|\alpha_1|$.

$$(9.9) \quad \zeta_n \leq M_{n-1} \dots (M_2 (M_1 \zeta_1 + G V_1) + G V_2) \dots + G V_{n-1} .$$

When $d_i \rightarrow 0$,

1. $G \rightarrow 0$ then equation (9.9) tend to $\zeta_n \leq M_{n-1} \dots M_2 M_1 \zeta_1$.
2. $M_k \rightarrow \begin{pmatrix} 1 & l_k \\ 0 & 1 \end{pmatrix}$ then, $M_k \dots M_2 M_1 \rightarrow \begin{pmatrix} 1 & \sum_{i=1}^{k-1} l_i \\ 0 & 1 \end{pmatrix}$.

From the two previous points, we obtain that

$$|\beta_i| \leq |\beta_1| + |\alpha_1| (a_i - a_1) + O\left(\sum_{i=1}^n d_i\right) .$$

Using (9.6), we have $|\alpha_1| (a_i - a_1) \leq (l_b/2 + \nu l_b^2/(2l)) \sum_{i=1}^n d_i$, and previous inequality become, $\forall i \in \{1, \dots, n\}$

$$(9.10) \quad |\beta_i| \leq |\beta_1| + O_1\left(\sum_{i=1}^n d_i\right) .$$

Remember that we have seen at the beginning that $\beta_1 = 0$, (9.10) show that γ^g tend to γ^i . Since this convergence occurs independently of ϕ_1 , we obtain the convergence of the γ_{max} curve.

9.4. Inline - magnetic convergence. We want to show in this part, the convergence of an inline solution to the magnetic approximation when $d_i \ll 1$. We already know that in this case the γ_{max} curve for the general current feed and inline feed tend to be equal. By this way, we show that for all ν , the γ_{max} curve of Eq.(4.1) tends to the magnetic approximation when $d_i \ll 1$.

We know that the magnetic approximation is given by $f(x) = Hx + c_{max}(H)$. Notice that c_{max} does not depend on the value of γ , see (4.11). We are going to

compare the magnetic approximation and the inline current feed solution for the same geometry. We proceed as in the previous part, we choose $\phi_1 = Ha_1 + c_{max}$. Remember that in the inline case, ϕ is a linear function by parts. $\forall x \in]a_i, a_{i+1}[$,

$$P_{i+1}(x) = (d_i \sin(P_i(a_i)) + P'_i(a_i))(x - a_i) + P_i(a_i).$$

Let us define:

$$\begin{aligned} \alpha_i &= P'_i(a_i) - f'(a_i) = P'_i(a_i) - H, \\ \beta_i &= P_i(a_i) - f(a_i). \end{aligned}$$

We obtain that $\alpha_1 = -\gamma/2$, $\beta_1 = 0$ and for a n junction circuit $\alpha_{n+1} = \gamma/2$. We estimate α_{i+1} :

$$\alpha_{i+1} = d_i \sin(P_i(a_i)) + P'_i(a_i) - H = d_i \sin(P_i(a_i)) + \alpha_i,$$

we obtain, $\alpha_{i+1} = \sum_{j=1}^i d_j \sin(P_j(a_j)) + \alpha_1$, thus

$$(9.11) \quad |\alpha_{i+1}| \leq \sum_{k=1}^n d_k.$$

We write β_{i+1} :

$$\begin{aligned} \beta_{i+1} &= (d_i \sin(P_i(a_i)) + P'_i(a_i))(a_{i+1} - a_i) + P_i(a_i) - Ha_{i+1} + b, \\ &= (d_i \sin(P_i(a_i)) + P'_i(a_i) - H)(a_{i+1} - a_i) + P_i(a_i) - Ha_i + b, \\ &= \alpha_{i+1}(a_{i+1} - a_i) + \beta_i. \end{aligned}$$

Thus if $\beta_1 = 0$ then

$$(9.12) \quad \beta_i = \sum_{k=1}^{i-1} \alpha_{k+1}(a_{k+1} - a_k).$$

Now using the bounds on the α 's and bounding the l_i 's we get

$$(9.13) \quad |\beta_i| \leq nl_b \sum_{k=1}^n d_k.$$

This shows that the γ_{max} of Eq.(4.1) tends to the magnetic approximation when $\sum_{k=1}^n d_k$ tends to 0.